Proceedings of ICFDP9:
Ninth International Congress of Fluid Dynamics & Propulsion
December 18-21, 2008, Alexandria, Egypt

ICFDP9-EG-218

A TWO-FLUID MATHEMATICAL MODEL FOR GAS-LIQUID FLOWS IN PROTON EXCHANGE MEMBRANE FUEL CELLS

Mohsen Abou-Ellail/Cairo University, Cairo, Egypt, email:abouellail@hotmail.com

S.H. Chan/ Fuel Cell Center, Yuan Ze University, Taiwan

Timothy W. Tong/George Washington University, Washington DC, USA

Karam R. Beshay/Cairo University, Cairo, Egypt

ABSTRACT

The present work considers a two-fluid mathematical model for the gas-liquid flow in PEM fuel cells. One fluid represents the continuous gas phase flowing through the layers of the fuel cell. For this fluid, the governing equations of momentum, energy, mass continuity and species mass fractions, are considered with additional inter-fluid exchange source terms. The second fluid represents the dispersed liquid phase flowing inside the layers of the fuel cell. The dispersed fluid is made up of small droplets in the gas channels and flowing layers of water over the particles of the porous media. The flow of the creeping water layers are controlled mainly by the capillary pressure and the wetability of the solid particles. As the thickness of the water layers increase, the electrochemical reactions will eventually vanish, thereby limiting the produced cell electric current. The mean droplet size of the flowing liquid, in the gas channels, is computed based on a simplified model for liquid jet disintegration by cross gas flow. This model is based on the balance of drag, viscous and surface tension forces acting on the droplets about to issue from the pores of the GDL. In order to obtain complete performance results, the computations are repeated for decreasing cell potentials until the limiting current is reached. The present results show that the liquid water spreads out from the end section of the cathode gas diffusion layer until most of the GDL is wet just before the limiting current is reached. The obtained two-fluid and single-phase simulations are compared with the corresponding experimental and numerical data available in the literature. The 2-fluid model shows that the blocking effect of the liquid phase starts to dominate, for cell voltage less than 0.7 V; in this case, the flowing 2-phase flow produces faster decrease in cell voltage as the loading electric current increases. This phenomenon was partially hindered by the LHF model but essentially bypassed by the single phase simulations. For voltages higher than 0.7, the 2-fluid model results are in better agreement with the experimental data.

KEYWORDS:

Two phase flow, fuel cell, proton exchange membrane, mathematical model.

INTRODUCTION

The PEM fuel cell works under low temperatures and hence is suitable for the automotive industry. The produced water vapor in the vicinity of the membrane can thus condense to liquid water, if the water mass fraction is higher than the saturation value corresponding to the local temperature. In this case the flowing fluid inside the layers of the PEM fuel cell is a 2-phase flow. The present two-fluid model treats each phase separately. In this case each fluid (phase) can have different velocity at the same computational node. Therefore, separate governing conservation equations are solved for each fluid, namely the gas-phase fluid and the liquid phase fluid. The resulting governing equations for momentum and species mass fractions together with the phase potential and mass continuity equations are solved iteratively using a two-fluid SIMPLE algorithm. In the present work the two fluids could be flowing in the porous media of the fuel cell, or in the gas channels, although most of the liquid phase is inside the pores of the cathode. One solution domain is superimposed over all the layers of the PEM fuel cell with appropriate boundary conditions applied at inlet, exit and sidewalls of the fuel cell. Special care is devoted to the electric phase potential, 'Poisson-type', equation boundary condition to prevent any escape of protons through the gas diffusion layers(GDL) and

simultaneously insuring a non-singular matrix of finite-difference coefficients (Chan et. al. [1]).

The computed two-fluid (2-phase) and single-fluid (1-phase) simulations are compared with experimental data (Ticianelli [2]).

MATHEMATICAL MODEL

In this section the governing equations for the two-fluid model are presented. The equations are based on a gaseous continuous fluid and a dispersed liquid fluid. If the liquid phase existed in the gas channels, it will assume the form of small droplets. However, most of the liquid will be in the fuel cell porous media in the form of flowing layers, over the solid matrix, acted upon mainly by capillary forces (Wang et al [3], Pasaogullari and Wang [4]). However, the present model offers separate conservation equations for the momentum of each fluid with inter-fluid exchange source terms (Chan and Abou-Ellail [5,6]). It should be mentioned here that although the flow is a two-phase flow, it may need a 3-fluid model to describe the case where the capillary flow and droplet-gas flow exist in the same computational micro space in the porous media.

Two-Fluid Model Equations

With the above assumptions, the mass continuity equations for the gas and liquid phases can contain extra source terms for condensation and/or evaporation, depending on the local water saturation conditions. Therefore, the two-fluid model mass continuity equation for the gas-phase can be written, for porous media, (Chan and Abou-Ellail [5,6], Gurau et. al. [7]) as:

$$\frac{\partial(\varepsilon\alpha_g\rho_g)}{\partial t}+\frac{\partial(\varepsilon\alpha_g\rho_g u_i)}{\partial x_i}=m_v-m_c \qquad (1)$$

and for the liquid-phase fluid, the continuity equation reads

$$\frac{\partial(\varepsilon\alpha_l\rho_l)}{\partial t}+\frac{\partial(\varepsilon\alpha_l\rho_l v_i)}{\partial x_i}=m_c-m_v \qquad (2)$$

Where, ε is the porosity; u_i is the gas-phase velocity; v_i is the liquid-phase velocity in direction i ; ρ is the density; α is the volume fraction of each phase and subscripts l and g denote liquid and gas phases, respectively; m_c and m_v are condensation and evaporation rates of H_2O per unit volume of physical space, respectively. In the present work, the evaporation rate will be neglected. This entails the assumption of uniform fuel cell temperature, as hypothesized by Wang et al [3]. Moreover, the studied PEM fuel cell uses fully humidified air (100% relative humidity) in the cathode with unlikely evaporation of any produced water. In this case the condensation rate m_c would essentially be equal to the production rate of H_2O by electro-chemical reactions; however, if the local relative humidity falls below 100% then m_c will be less than H_2O production rate by the amount which remains in the gas phase. In addition to the above equations, the overall continuity must be included, namely

$$\alpha_l+\alpha_g=1 \qquad (3)$$

It should be noted that according to the 2-fluid model, the two fluids share the local physical space, such that each fluid occupies a fraction of the volume equivalent to its volume fraction. Therefore, all conservation equations of each fluid must properly include these volume fractions either explicitly or implicitly, as can be seen from the above and following governing equations (Chan et. al. [5,6]).

In a PEM fuel cell, the gas-liquid flow is essentially laminar. The two-fluid governing equations for heat, mass, species mass fractions and momentum transfer can be written in a general form for the gas-phase, as follows (Chan and Abou-Ellail [5,6] Gurau et. al. [7], Zhou and Liu [8], Sukkee, et. al. [9]):

$$\frac{\partial(\varepsilon\rho_g\alpha_g\psi)}{\partial t}+\frac{\partial(\varepsilon\rho_g\alpha_g u_i\psi)}{\partial x_i}-\frac{\partial}{\partial x_i}(\varepsilon\rho_g\alpha_g\frac{\nu}{\sigma_\psi}\frac{\partial\psi}{\partial x_i})=S_\psi \qquad (4)$$

Similarly, for the 2-fluid liquid-phase governing equations for mass and momentum can be written as:

$$\frac{\partial(\varepsilon\rho_l\alpha_l\psi)}{\partial t}+\frac{\partial(\varepsilon\rho_l\alpha_l v_i\psi)}{\partial x_i}-\frac{\partial}{\partial x_i}(\varepsilon\rho_l\alpha_l\frac{\nu}{\sigma_\psi}\frac{\partial\psi}{\partial x_i})=S_\psi \qquad (5)$$

Where, ψ, in equations (4) and (5), stands for u_j, absolute temperature T and species mass fractions Y_k , for the gas-phase, and v_j for the liquid-phase,. The time is denoted by t, while k=1, 2, 3 & 4 stands for species H_2, O_2, H_2O and H^+ respectively. It should be mentioned here, that equation (4) can also be used for electrical phase potential ϕ if ε and u_i are set equal to 1.0 and zero respectively. σ_ψ is the Prandtl/Schmidt number, for ψ. S_ψ is the source term corresponding to the dependent variable ψ, being solved for. Expressions for S_ψ and σ_ψ , of the liquid and gas phases, are given in Table 1 for each dependant variable ψ. The momentum source terms are written here such that they apply to the fuel cell in a general way, with some terms vanishing naturally in particular layers as a result of the local physical conditions. The capillary pressure p_c, which appears in the liquid-phase momentum source terms, can be computed for a hydrophilic porous media from the following relation (Wang et. al. [3])

$$p_c=\sigma(\varepsilon/K)^{1/2}\left[\ 1.417(1-s)-2.120(1-s)^2+1.263(1-s)^3\ \right] \qquad (6)$$

Where, σ is the water-gas surface tension and s is the liquid water saturation, which can be computed from the local liquid-phase volume fraction α_l and the local physical properties of the flowing mixture. Both s and α_l are equal to unity or zero, if the local flow is a pure liquid or pure gas respectively.

Moreover, the liquid and gas permeabilities are related to the water saturation, s, by the following relations (Wang et. al. [3])

$$K_l=s^3K \quad \text{and} \quad K_g=(1-s)^3K \qquad (7)$$

The drag force, exerted by the gas-phase on the liquid-phase, per unit volume of liquid-phase (F_{D_j} in Table 1) can be

expressed as a function of the slip velocity (Chan and Abou-Ellail [5,6]), namely

$$F_{D_j} = f_D(u_j - v_j) \quad (8)$$

Where, f_D is a drag function that is directly proportional to the gas viscosity and the square of the surface area per unit volume of the liquid-phase, i.e. $1/D^2$ for dispersed droplet flow, (Chan and Abou-Ellail [5,6]). The last two terms in the momentum source terms, in Table 1, are included to account for 'convective' inter-phase transport due to phase change in the PEM fuel cell. If the liquid volume fraction increases considerably, the dispersed phase will become the flowing bubbles with a mean diameter D.

The present computational procedure is based on the solution of equations (4) and (5) inside the PEM fuel cell treated as one continuous solution domain. In this case, ε assumes values appropriate to the different layers of the PEM fuel cell, e.g. ε=1.0 in the gas channels and for the GDL, catalyst layers and membrane ε is less than 1.0 according to the local values. Similarly with the volume fractions of the liquid and gas phases, however small any of them may be. Moreover, the inter-phase mass exchange affects also the source term of the water vapor mass fraction, as given in Table 1. In the present work, all gases are assumed insoluble in the liquid water, and hence the liquid-phase in the fuel cell is pure.

Auxiliary Equations

The complex flow of gas, liquid, protons and electro-chemical reactions in PEM fuel cells requires additional relations to specify the interlinking of these phenomena. The open-circuit potential E_o (in volts) represents the theoretical maximum cell potential. It can be computed directly from the Gibbs free energy change across the fuel cell (ΔG), when the current density approaches zero (Barbir [10]):

$$E_o = (-\Delta G)/(nF) \quad (9)$$

Where, n is the number of electrons per molecule of the fuel (n=2 for hydrogen).

Under working conditions, the PEM fuel cell will have a potential less than Eo by the total polarization losses, which is dependent on the load electric current density. The open-circuit potentially E_o is only used as a reference value for the cell potential at zero current density.

In the cathode and anode catalyst layers, the transfer current densities Jc and Ja are given by Burtler-Volmer equations (Gurau et. al.[7], Zhou and Liu [8]):

$$J_c = (1-\alpha_l) a_{jo}^{ref} \left(\frac{X_{O_2}}{X_{O_2 ref}}\right) \left[\exp\left(\frac{\alpha_a^c F \eta_c}{RT}\right) - 1/\exp\left(\frac{\alpha_c^c F \eta_c}{RT}\right)\right] \quad (10)$$

$$J_a = (1-\alpha_l) a_{jo}^{ref} \left(\frac{X_{H_2}}{X_{H_2 ref}}\right)^{1/2} \left[\exp\left(\frac{\alpha_a^a F \eta_a}{RT}\right) - 1/\exp\left(\frac{\alpha_c^a F \eta_a}{RT}\right)\right] \quad (11)$$

Where, η is the overpotential in volts; F is faraday constant (=96487 C/mol); X is mole fraction. Superscript (or subscript) ref stands for reference conditions. The numerical values of the transfer coefficients $\alpha_a^c, \alpha_c^c, \alpha_c^a$ & α_a^a and the reference exchange current density α_{Jo}^{ref} are given by Gurau et. al. [7].

In the present work, the phase potential is referenced from the anode catalyst layer-GDL interface potential. Subtracting the open-circuit potential from the actual local phase potential does this. Hence, the phase potential on the cathode catalyst layer-diffuser interface represents the total polarization of the fuel cell at a particular loading electric current. Moreover, the overpotential in the anode and cathode catalyst layers can be computed as,

$$\eta_a = \phi_a - \phi \quad (12)$$

$$\eta_c = \phi_c - \phi \quad (13)$$

Where, ϕ_a and ϕ_c are the phase potentials at the anode catalyst layer-GDL interface and cathode catalyst layer-GDL interface, respectively. The overpotential computed from the above equations is solely dependent on the local phase potential for a fixed fuel cell potential. With the phase potential referenced from the anode catalyst layer-GDL interface, ϕ_a is essentially equal to zero, while the overpotential is positive in the anode catalyst layer and negative in the cathode catalyst layer. Moreover the value of ϕ_c will be fixed to represent a given working cell potential that is also equivalent to defining a fixed value for the average current density (Gurau et. al. [7]).

Jc and Ja, in equations (10) and (11), represent the source terms for the potential ϕ equation in the catalyst layers. They also contribute to the source terms for mass fraction equations of O_2, H_2, H_2O and H^+ (Sukkee and Wang [11]).

The ionic conductivity σm in a 117 Nafion proton exchange membrane can be expressed as (Gurau et. al. [7], Zhou and Liu [8]):

$$\sigma_m(T) = [0.005139 \cdot a - 0.00326]\exp[1268(\frac{1}{303} - \frac{1}{T})] \quad (14)$$

Therefore σϕ, of the phase potential governing equation, can be computed as:

$$\sigma_\phi = \rho_g v_g / \sigma_m \quad (15)$$

In equation 14, a is the water vapor activity defined as:

$$a = \frac{X_{H_2O} P}{P^{sat}} = \frac{X_{H_2O}}{X_{H_2O}^{sat}} \quad (16)$$

Here, X_{H_2O} is the mole fraction of the total H_2O present in the local mixture of gas and liquid.

The saturation pressure Psat can be estimated from the empirical equation (Sukkee et al.[9]):

$$\text{Log}_{10}P^{sat}=-2.1794+0.02953(T-273)-9.1837\text{x}10^{-5}(T-273)^2+1.4454\text{x}10^{-7}(T-273)^3 \quad (17)$$

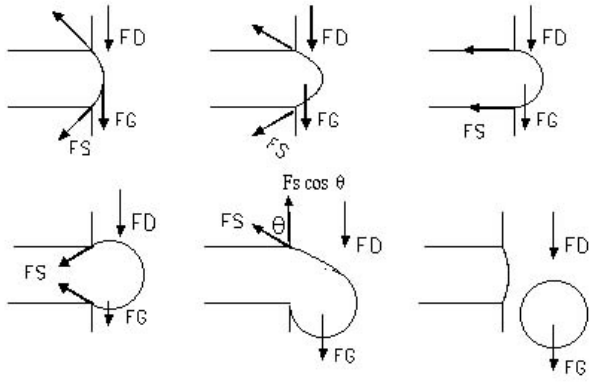

Fig. 1 Proposed droplet formation mechanism at the GDL-gas channel interface.

The mean droplet size of the flowing liquid, in the gas channel, is computed from the balancing of the drag force and gravitational force on one side, and the surface tension forces acting on the liquid emerging from the pores of the gas diffusion layer. Each pore is assumed to produce droplets separated from the neighboring pores, as shown schematically in Fig.1. As the liquid continues to flow through the pores, the emerging droplets stay attached to the pore rims, until the drag and gravity forces overcome the surface tension forces. This will take place when the growing droplet size is infinitesimally larger than D given by the following equation (for a fixed value of θ)

$$\rho_l \frac{\pi D^3}{6} g_j + \rho_g C_D \frac{\pi D^2}{4} \frac{(u_j - v_j)^2}{2} = \sigma d \cos\theta \quad (18)$$

Where, D is the droplet diameter and d is the average pore size; θ is the acute angle between the surface tension force and the x direction at the droplet leading edge; g_j is the acceleration of gravity in direction j=1(axial direction) and C_D is calculated as the drag coefficient for solid spheres at low Re as:

$$C_D = \frac{24}{\text{Re}_j} \quad (19)$$

Where Re_j is the axial droplet Reynolds number based on the absolute axial relative velocity between the gas and the liquid. The angle α is also affected by the growing droplets, in such a way to balance the left hand side of equation (18). The effect is such that the surface tension force on the leading edge rotates toward the axial direction as α decreases to its possible minimum value. Equation (18) indicates that the liquid droplet diameter is inversely proportional to the air velocity inside the GDL. Similar behavior was confirmed analytically and experimentally by Zhang et al. [12].

Finite Difference Equations

The PEM fuel call is overlaid with a finite grid of nodes. At each nodal point, the general governing partial differential equations for the two fluids are formally integrated over a control volume surrounding this nodal point. The faces of the control volume bisect the distances between the particular node and the four nearest neighbor nodes. The formal integration is performed with due care to preserve the physical meaning and overall balance of each dependent variable. The final form of the finite difference equations are as follows:

$$(\Sigma (A_n) - S_p)\ \psi_p = \Sigma\ (A_n \psi_n) + S_u \quad (20)$$

Where, ψ stands for any of the dependent variables u_j, v_j, α_l, T, species mass fractions, phase potential or pressure correction used to satisfy mass continuity and momentum equations, of the two fluids, simultaneously. The summation Σ is over the n four neighbors of a typical node p. The above finite difference coefficients A_n are computed using the upwind method, such that these coefficients are always non-negative to give the proper effect of convection and diffusion. S_p and S_u are the coefficients of the integrated source term, as given in Table 1, over the control volume surrounding node p. It should be mentioned here that, only diffusion is included in A_n when the phase potential equation is solved, to reflect the absence of convection as indicated in Table 1. Both the pressure correction equation, which is a modified form of the mass continuity equation, and the phase potential equation are Poisson–type equations that require special treatment of boundary conditions (Chan et al [13]). Since the membrane is impermeable to both the hydrogen and the oxygen, an infinitely large linear source term, with a negative sign, is used in the membrane for these gases to prevent the diffusion of H_2 and O_2 into the membrane. The result is that the hydrogen and oxygen never mix inside the fuel cell and only water and protons diffuse through the membrane.

In the present work, a 2-fluid SIMPLE algorithm is adopted (Chan et. al. [5,6]). The modified SIMPLE algorithm is based on a pressure correction equation obtained by adding equations (1) and (2) of the 2-fluid continuity equations. The obtained equation has the advantage of removing any mass source terms due to mass exchange between the two fluids. In this case the liquid-phase volume fraction, α_l, is computed from equation (2), while α_g is simply calculated from equation (3). The solution of the 2-fluid pressure correction equation, gives pressure perturbations that are used to correct simultaneously the momentum based u_j and v_j such that the mass continuity equations are satisfied.

Boundary Conditions

The present solution procedure is based on one solution domain. Therefore, the boundary conditions must be imposed

on the inlet section, sidewalls and exit section of the fuel cell depicted in fig. 2. At the inlet section all variables have fixed values except the phase potential which has zero normal gradient. The inlet gas-phase axial and transverse velocity components are 0.32 and 0.0 m/s, while the inlet liquid-phase velocity is 0.0 m/s. The inlet temperature, gas-phase and liquid-phase volume fractions are 353 K, 1.0 and 0.0, respectively. The inlet species mass fractions can easily be computed knowing that the anode is fed by pure hydrogen while the cathode is supplied with saturated humidified air (100% relative humidity). The sidewalls are impermeable; hence the normal gradient of all dependent variable is equal to zero, except the velocity components themselves vanish at the walls. At the exit section all dependant variables, except the velocity components, have zero normal gradients. However, the velocity components, at the exit section, have zero gradients in the gas channels and zero value everywhere else. Additional constrains must be imposed on the finite-difference equations of the phase potential, as explained below, to remove inherent singularity of Poisson-type equations (Chan et al. [13,1]). The fuel cell is aligned with its axis along the gravitational acceleration; therefore, g_j, in equation (18) is equal to 9.81 m/s^2 .

Treatement of Phase Potential Boundary Conditions

The boundary condition of the phase potential governing equation is unique. In order to prevent the hydrogen protons from entering or leaving the boundaries of the solution domain of the phase potential, zero gradients must be applied at the boundaries (Gurau et al [7]). However, this would create a singular matrix of finite-difference coefficients, with infinite solutions, due to the Poisson-type nature of the phase potential equation. Instead, defining fixed values of the phase potential at the anode, cathode or both catalyst layer-GDL interfaces can solve the problem of singularity. However, it will create another problem, namely the inflow or outflow of protons at the modified boundaries, where the normal gradient of ϕ is not zero. The solution offered here is to specify a fixed value and zero gradient for ϕ along the catalyst-GDL interfaces, as can be seen from Fig.3. This is done by defining special linear source terms large enough to dominate the finite-difference equations of the phase potential, as given by equation (20), at the designated boundaries. At the cathode catalyst layer-GDL interface, the source term coefficients at node (i , j_c) may be defined as

$$S_u(i, j_c) = G(\phi_c) \quad (21)$$

$$S_p(i, j_c) = -G \quad (22)$$

Where, G is a sufficiently large number (in the order of 10^{30}). Similar relations can be written for node (i , j_{c+1}) source term coefficients. It can be seen that, when Eqs. 19 & 20 are substituted in Eq.18, the phase potential will be fixed at a value of ϕ_c at the two nodal points across the cathode catalyst layer-GDL interface satisfying concurrently a zero gradient at the same interface. The above argument applies also to nodes (i,j_a-1) and (i,j_a) of the anode, where the phase potential has to be fixed at a value of $\phi_a = 0.0$ and zero transverse gradient of ϕ, as depicted in Fig.3. At the inlet and exit sections of the fuel cell, a simple zero axial gradient boundary condition, for ϕ, is applied.

SOLUTION PROCEDURE

The solution procedure is based on the line-by-line alternating direction TDMA algorithm. The difference equations (Eq.18) for each dependant variable are modified at the outer boundary conditions of the PEM fuel cell to incorporate the conditions imposed there. The solution is then obtained using the above algorithm. The solution is then repeated for all the dependant variables. The above loop of computations is then repeated a number of times, until complete conversion is obtained. These iterations are needed since the governing equations are elliptic and strongly coupled in nature with effects propagating in all directions especially for the pressure correction and the phase potential. Figure 3 depicts the PEM fuel cell studied in the present work. The length of the PEM fuel cell is 7.62 cm while the width of each gas channel, of the anode or the cathode is 0.0762 cm. The gas diffusion layer (GDL) thickness is 0.0254 cm, while the thickness of the catalyst layer is 0.00287 cm for the anode or the cathode. The membrane thickness is 0.023 cm. The porosity of the GDL is 0.4 while that of the membrane is 0.28. Moreover, the effective porosity of the catalyst layer is 0.14. The basic geometrical and physical data of the computed PEM fuel cell are given in Table 2.

PRESENTATION AND DISCUSSION OF RESULTS

Two-fluid and single-phase numerical simulations, for a PEM fuel cell working at air pressure of 5 bar and fuel pressure of 3 bar at 353 K (Gurau et. al. [7], Sukkee, et.al. [9]), were obtained. The inlet gas velocity is 0.35 m/s, while the liquid-phase inlet velocity is equal to zero. A grid of 60X60 is used, which required 1100 iterations for complete conversion. Special care is devoted to the boundary condition of the phase potential equation to satisfy zero gradient as well as specified working current density for each simulation (Abou-Ellail, [14]). The droplet diameters are computed from equation (18), using equation (19) to obtain the drag coefficient, at each axial grid node along the GDL-gas channels interface. For a cell potential of 0.8 V, the droplet diameter ranges between 150 to 170 microns. Chen [15] measured droplets of the order of 100 microns in similar conditions, while Zhang et al. [12] measured higher values for the water droplet diameter. A mean value of 160 micron is used for the computation of the drag forces acting on the liquid phase by the flowing continuous gas phase. These drag forces appear in the momentum equations of both phases with opposite signs, as shown in Table (1).

The transverse profiles of the axial velocities of the liquid-phase and gas-phase, at 0.002 m from the inlet section, are depicted in Fig.4, at a cell potential of 0.8 V. The gas-phase

axial velocity is two orders of magnitude higher than the liquid-phase axial velocity. The transverse profiles of the gas-phase and liquid phase transverse velocities are shown in Fig.5, for an axial distance of 0.002 m from the inlet section. Here, the magnitude of gas-phase transverse velocity is also roughly two orders of magnitude higher than the transverse liquid-phase velocity. It can be seen from Fig.5, that in the cathode the liquid-phase is moving outwardly, from the fuel cell centerline, while the gas-phase is flowing inwardly. This is because the gas-phase is driven by the gas negative pressure gradient while it seems that the main driving force of the liquid is the capillary positive pressure gradient The sign difference between the effect of the gradients of p and p_c results from the liquid pressure being equal to ($p - p_c$), as explained by Wang et. al. [3] and Pasaogullari and Wang [4]. Similar liquid water movements in the cathode GDL was predicted by Wang et al. [3] and by Zhang et al. [12]. However, they used a hybrid scheme, where the liquid velocity is computed from Darcy's equation while the gas-liquid flow is calculated from the momentum balance equation of the mixture. The transverse profiles of mass fractions of H_2O vapor, H_2 and O_2 are depicted in Fig.6, for x = 0.002 m and cell potential of 0.8 V, obtained with the two-fluid model. At this section, the flowing gases, in the cathode gas channel, are essentially saturated with water vapor, while the gases in the anode have relative humidity less than 100 %. The water vapor in the anode must have come by diffusion from the cathode high water vapor content. The two-fluid liquid volume fraction (α_l) profiles, along the transverse distance y, are shown in Fig.7 at sections 0.001, 0.025, 0.04 and 0.06 m from the inlet section, for 0.8 V cell voltage. The liquid water volume fraction increases ten times as the flow moves from x = 0.001 m to x =0.06 m near the exit section. The maximum liquid water volume fraction, which occurs at the cathode catalyst layer-membrane interface, at cell potential of 0.8 V, is 0.0035, which is equivalent to about 0.4 mass fraction. However, the liquid volume fraction in the anode is extremely small. For cell potentials lower than 0.8, i.e. current densities higher than 0.8 A/cm2, the maximum liquid water volume fraction increases considerably, producing the inevitable partial blocking of the pores of the cathode. The present values of the liquid volume fraction are considerably higher than those predicted by Chan et. al, [1]. The difference is attributed to the inadequacy of the LHF model to simulate the liquid water management in PEM fuel cells.

Figure 8 depicts transverse profiles of the phase potential, taking a reference value at the anode and a cell potential of 0.8 V, for the PEM fuel cell. Examining the phase potential profiles of Fig.8 shows clearly the required effect on these profiles, as dictated by the special treatment of ϕ boundary condition. The transverse gradients of the phase potential, at the cathode catalyst layer-membrane interface, are used to compute the electric current density (I) (Gurau et. al. [7], Zhou and Liu [8]). The single-phase and two-phase cell potential versus current density comparisons with experimental data of Ticianelli, et. al. [2], show clearly the importance of including the liquid phase in any practical simulations of PEM fuel cells at high current densities, as depicted in Fig.9. The two-fluid cell potential decreases faster than that for single-phase simulations, especially for current densities higher than 1.0 A/cm^2. This fast decrease in the cell potential is caused mainly by the high liquid volume fraction, at very low mobility, generated in the fuel cell.

The two-fluid gas and liquid water velocity vector plots, in the cathode gas diffusion and catalyst layers, are depicted in Fig.10 a and b, for 0.8 V cell potential. The cathode membrane-catalyst-layer interface is near y=0.00128 m, while the cathode GDL-gas-channel interface is at y=0.00130 m. The gas velocity vectors, in Fig.10a, show a continuous flow toward the membrane-catalyst-layer interface, while the liquid water moves in the opposite direction, at a much lower pace, toward the gas channel-GDL interface, as shown in Fig.10b. Since the air entering the cathode has a relative humidity of 100%, liquid water spreads essentially all over the GDL and catalyst layer. The liquid water velocity is much higher, in the vicinity of the fuel cell exit section, than near the inlet section. This is indicative of high capillary pressure gradient near the exit section. The liquid water volume fraction contours, in the cathode gas channel and gas diffusion layer, are depicted in Fig.11, close to the limiting current at a cell potential of 0.22 V. The water volume fraction increases considerably along the cathode. It reaches about 0.25 near the cathode exit section. The accumulation of liquid water, in the cathode, causes the cathode catalytic layer to lose 25 percent of its electro-chemical effectiveness, in the vicinity of the exit section. Moreover, the gas channel exit area is also reduced by similar factor. Alternatively, it is possible to hypothesize that the cathode exit section is fully blocked 25 percent of the time and unblocked at other times.

CONCLUSIONS

The present single phase and two-fluid simulations, of the PEM fuel cell, show that the electric current density is under predicted for 1-phase, while the 2-fluid properly computes the performance of the parallel geometry fuel cell for the range of the cell potential reported in the literature. For electric current densities higher than 0.8 A/cm^2, the two-fluid model predicts appreciable blocking effects of the liquid water in the catalyst layers and GDL. Consequently, the cell potential starts to decline significantly at higher current densities. On the other hand, the single-phase simulations could not predict any faster decline of the cell potential, for higher values of the electric current density.

The droplets in the gas channel are formed at the GDL-gas channel interface pores due to the drag, gravity and surface tension forces balance. The droplet diameter, in the gas channels, ranges between 150 to 170 microns. The velocity vectors of the liquid water in the cathode GDL are essentially in opposite direction to the gas-phase velocity vectors. This results mainly from the effect of the capillary pressure, causing

the liquid pressure to increase at the cathode catalyst layer-membrane interface relative to that at the cathode gas channel-catalyst layer interface. Moreover, the absolute value of the liquid-phase velocity is approximately two orders of magnitude less than the co-flowing gas-phase in the cathode GDL and catalyst layer. The liquid water moves faster in the vicinity of the fuel cell exit section which must be due to the higher capillary pressure gradient in this zone. In the gas channels the liquid droplets flow much slower than the gas phase, giving rise to high slip velocities between the two phases.

The liquid water volume fraction increases appreciably for high electric current density, due to the increased blocking effects and decreased water mobility. It reaches 0.25 at the cathode exit section as the current density approaches its limiting value. This phenomenon predicts the onset of water flooding of the fuel cell electrodes. Finally, the computed phase potential transverse profiles have the right characteristics that were only possible through the special treatment of the boundary condition of the Poisson-type phase potential transport equation.

NOMENCLATURE

a	water activity
D	mass diffusivity of species, m^2/s, also, droplet diameter, m
d	mean pore size, m
F	Faraday constant, 96487 C/mol
G	a very large number (1.0E+30)
h	gas enthalpy, J/kg
I	current density, A/ cm^2
j	transfer current, A/ m^2
K	permeability, m^2
k	chemical species k
L	cell length, cm
M	molecular mass, kg/ Kmole
P	pressure, Pa
R	gas constant, 8.314 J/mol· K
Re	droplet Reynolds number
S	source term in transport equations
t	time, s
T	temperature, K
u_i	gas-phase velocity component in i direction, m/s
v_i	liquid-phase velocity component in i direction, m/s
V	cell potential, V
X	mole fraction
x_i	space coordinates

Greek letters

α	transfer coefficient, volume fraction
ε	porosity
κ	ionic conductivity, S/m
ψ	general dependant variable
Φ	phase potential, V
μ	viscosity, kg/m· s
ρ	density, kg/m^3
σ	Prandtl/Schmidt number, surface tension (N/m)
η	overpotential, V

Superscripts

c	cathode
eff	effective value
m	membrane phase
sat	saturation value

Subscripts

a	anode
c	cathode, capillary
eff	effective value
g	gas phase
i	direction i
j	direction j
in	inlet
l	liquid phase
o	open circuit
ref	reference value
ψ	relevant to general dependant variable
Φ	phase potential equation

REFERENCES

[1] S.H. Chan, T. Tong, M. Abou-Ellail, and K. R. Beshay, " A Two-Phase Flow Mathematical Model for Proton Exchange Membrane Fuel Cells with Enhanced Geometry," *Proceedings of the Fuel Cell Science, Engineering and Technology 2004*, ASME Conference, Rochester, N.Y., Paper # 2004-2447, pp. 23-29, 2004.

[2] E.A. Ticianelli, C.R. Derouin, and S. Srinvasan, "Localization of Platinum in Low Catalyst Loading Electrodes to Attain High Power Densities in SRE Fuel Cell", *J Electroanal. Chem.*, Vol. 251, p.275, 1988.

[3] Z.H. Wang, C-Y. Wang, and K.S. Chen, " Two-Phase Flow and Transport in the Air Cathode of Proton Exchange Membrane Fuel Cells," *Journal of Power Sources*, Vol. 94, pp. 40-50, 2001.

[4] U. Pasaogullari, and C-Y. Wang, " Two-Phase Transport and the Role of Micro-Porous Layer in Polymer Electrolyte Fuel Cells." *Electrochimica Acta*, Vol. 49, pp. 4359-4369, 2004.

[5] S.H. Chan, and M.M.M. Abou-Ellail, "A Multi-Fluid Model of Turbulence for Li-SF6 Submerged Combustion," *AIAA/SEA/ASME/ASEE 28th Joint Propulsion Conference*, Nashville, TN, paper # AIAA 92-3137, 1992.

[6] S.H. Chan, and M.M.M. Abou-Ellail, "A Two-Fluid Model for Reacting Turbulent Two-Phase Flows," *Journal of Heat Transfer, Transactions of the ASME*, Vol. 116, Number 2, pp 427-435, 1994.

[7] V. Gurau, H. Liu, and S. Kakac, "Two-Dimensional Model for Proton Exchange Membrane Fuel Cells", *AIChE J.*, Vol. 44, No. 11, pp. 2410-2422, 1998.

[8] T. Zhou, and H. Liu, "A General Three-Dimensional Model for Proton Exchange Membrane Fuel Cell", *J Trans. Phenomena*, Vol.3, No.3, pp.117-198, 2001.

[9] Um. Sukkee, C.-Y Wang, and K.S. Chen, "Computational Fluid Dynamics Modeling of Proton Exchange Membrane Fuel Cells", *J Electrochem. Soc.*, Vol. 147, No.12, p.4485, 2000.

[10] F. Barbir, "PEM Fuel Cells: Theory and Practice", *Elsevier Academic Press*, p. 21, 2005.

[11] Um. Sukkee, and C.Y Wang, "Three Dimensional Analysis of Transport and Reaction in Proton Exchange Membrane Fuel Cells", *Proc. ASME Fuel Cell Division-2000*, ASME Int. Mech. Eng. Congress & Exposition, 2000.

[12] F.Y. Zhang, X.G. Yang and C.Y. Wang, " Liquid Water Removal from a Polymer Electrolyte Fuel Cell," *Journal of the Electrochemical Society*, Vol. 153(2), pp. A225-A232, 2006.

[13] S.H. Chan, T. Tong, M. Abou-Ellail, and K. Beshay, "Numerical Simulation of the Performance of Proton Exchange Membrane Fuel Cells," *2003 Fuel Cell Seminar*, Miami, Fl, Paper # 218, pp 218-1 – 218-4, 2003.

[14] M.M.M. Abou-Ellail, "Prediction of Irregular Axi-Symmetric Combustor Aerodynamics and Convective Heat Transfer", *Numerical Methods in Lam. & Turbulent Flow*, Ed. C. Taylor el al, Pineridge Press, Swansea, pp 223-245, 1985.

[15] L.D. Chen, Private Communications, Iowa University, 2006.

.

Table 1 Source term and Prandtl /Schmidt number for dependent variable of equations (4,5)

ψ	σ_ψ	S_ψ	Comments
1	0	$m_v - m_c$	Gas-phase continuity equation
1	0	$m_c - m_v$	Liquid-phase continuity equation
u_j	1	$-\frac{\partial \alpha_g \varepsilon p}{\partial x_j} + \frac{\partial}{\partial x_i}\left[\rho_g \alpha_g \varepsilon \nu_g \left(\frac{\partial u_j}{\partial x_j} - \frac{2}{3}\frac{\partial u_k}{\partial x_k}\delta_{ij}\right)\right]$ $-\frac{\rho_g \nu \alpha_g \varepsilon^2}{K_g} u_j + \alpha_g \frac{k_\phi}{k_p} z_f c_f F \frac{\partial \phi}{\partial x_j} - \alpha_l \varepsilon F_{D_j}$ $+ m_v v_j - m_c u_j$	Gas-phase momentum equation The Darcy force term vanishes in gas channel ε = 1.0 & $k_{eff} = \infty$; the electro-kinetic force term vanishes in gas channel and GDL as $\frac{\partial \phi}{\partial x_j} = 0$.
v_j	1	$-\frac{\partial \alpha_l \varepsilon (p - p_c)}{\partial x_j} + \frac{\partial}{\partial x_i}\left[\rho_l \alpha_l \varepsilon \nu_l \left(\frac{\partial v_j}{\partial x_j} - \frac{2}{3}\frac{\partial v_k}{\partial x_k}\delta_{ij}\right)\right]$ $-\frac{\rho_l \nu \alpha_l \varepsilon^2}{K_l} v_j + \alpha_l \frac{k_\phi}{k_p} z_f c_{\ f} F \frac{\partial \phi}{\partial x_j} + \alpha_l \varepsilon F_{D_j}$ $- m_v v_j + m_c u_j + (\rho_l - \rho_g)\alpha_l \varepsilon g_j$	2-fluid model liquid-phase momentum equation. Last term represents the net force due to gravity and buoyancy. The capillary pressure vanishes in the gas channels; with gas pressure equals the liquid pressure.
y_{H2}	ν / D_{H_2}	$\begin{cases} -J_a M_{H_2}/(2F) \\ 0 \end{cases}$	In anode catalyst layer, where J_a is positive. In anode gas channel and GDL
y_{O2}	ν / D_{O_2}	$\begin{cases} J_c M_{O_2}/(4F) \\ 0 \end{cases}$	In cathode catalyst layer, where J_c is negative In Cathode gas channel and GDL
y_{H_2O}	ν / D_{H_2O}	$\begin{cases} -J_c M_{H_2O}/(2F) - m_c + m_v \\ 0 \end{cases}$	In cathode catalyst layer, where J_c is negative Zero H_2O production outside cathode catalyst layer
y_{H^+}	ν / D_{H^+}	$\begin{cases} J_a M_{H^+}/(F) \\ J_c M_{H^+}/(F) \\ \varepsilon_m z_{H^+} x_{H^+}\left(F/\bar{R}T\right) D_H + \frac{\partial}{\partial x_i}\left(\frac{\partial \phi}{\partial x_i}\right) \end{cases}$	Production of H^+ in anode catalyst layer consumption of H^+ in cathode catalyst layer In membrane only (if σ_m is uniform in membrane then) $\frac{\partial}{\partial x_i}\left(\frac{\partial \phi}{\partial x_i}\right) = 0$
H	P_r	$\begin{cases} (m_c - m_v)\Delta h_{evap} \\ (m_c - m_v)\Delta h_{evap} + \sigma_m \alpha_g \frac{\partial \phi}{\partial x_i}\frac{\partial \phi}{\partial x_i} \end{cases}$	Gas channels and GDL In membrane and catalyst layers ($-\sigma_m \frac{\partial \phi}{\partial x_i} = I_i$, while $\frac{\partial \phi}{\partial x_i}$ is the local gradient of phase potential).
ϕ	$\rho\nu / \sigma_m$	$\begin{cases} J_a \\ 0 \\ J_c \end{cases}$	Anode catalyst layer, $u_i = 0$ Membrane, $u_i = 0$ (no convection) Cathode catalyst layer, $u_i = 0$

Table 2 Basic physical parameters of PEM fuel cell

Physical Quantity	Value
Cathode pressure	5 bar
Anode pressure	3 bar
Inlet velocity u_i	0.35 m/s
Cell temperature	353 K
Relative humidity of inlet hydrogen	0.0 %
Relative humidity of inlet air	100%
Reference exchange current density × area of anode, aJ_a^{ref}	1000 A/cm^3
Reference exchange current density × area of cathode, aJ_c^{ref}	0.3 A/cm^3
Oxygen diffusivity in gas	5.2197E-06 m^2/s
Hydrogen diffusivity in gas	2.63E-06 m^2/s
Water vapor diffusivity at the anode side	0.733E-6 m^2/s
Water vapor diffusivity at the cathode side	0.49E-6 m^2/s
Dissolved oxygen diffusivity in active layer and membrane	2.0E-8 m^2/s
Dissolved hydrogen diffusivity in active layer and membrane	2.59E-10 m^2/s
Water-gas surface tension, σ	6.25E-2 N/m
Hydraulic permeability of membrane, k_p	1.8E-18 m^2
Permeability of GDL layer, K	1.76E-11 m^2
Electro-kinetic permeability, k_ϕ	7.18E-20 m^2
Fixed site charge, Z_f	-1
Faraday constant, F	96487 C/mol
Anodic transfer coefficient, α_a	2
Cathode transfer coefficient, α_c	2
GDL porosity, ε	0.4
Membrane porosity, ε_m	0.28
Membrane Volume fraction in the Catalyst layer, ε_{mc}	0.5
Fixed charge concentration, C_f	1.2E-3 mol/cm3
Gas channel length, L	7.62 cm
Gas channel width	0.0762 cm
Gas diffusion layer(GDL) width	0.0254 cm
Catalyst layer width	0.00287 cm
Membrane width	0.023 cm
GDL pore size (d)	0.001 cm

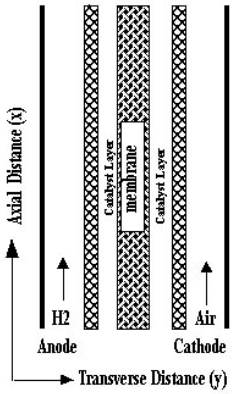

Fig. 2 The PEM fuel cell geometry

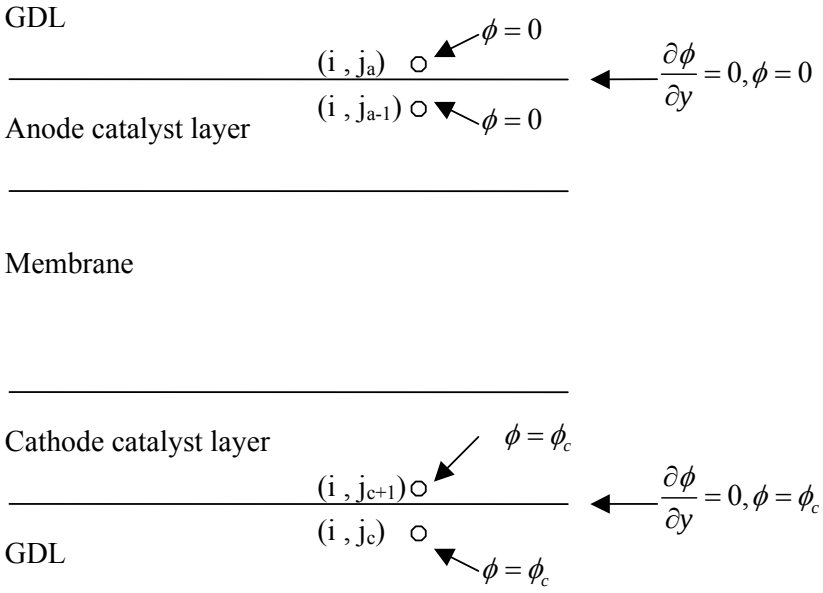

Fig. 3 Special treatment of boundary conditions for phase potential equation.

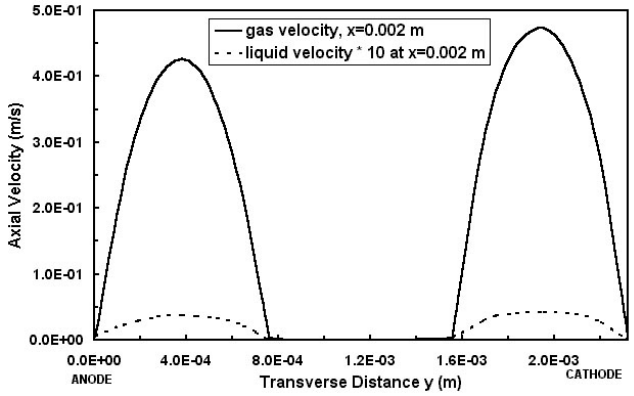

Fig. 4 Profiles of axial velocities of gas and liquid water in PEM fuel cell at 353 K.

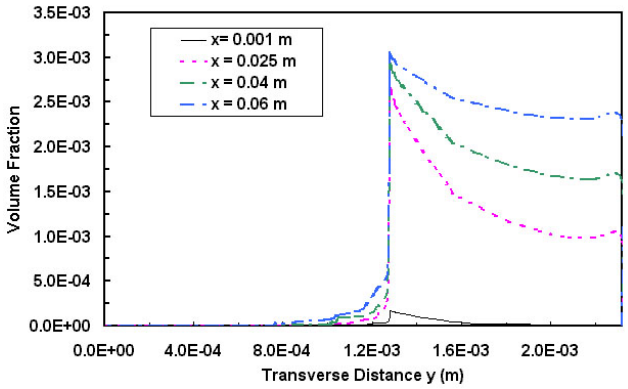

Fig. 7 Transverse profiles of liquid volume fraction for cell potential = 0.8 V and T=353 K in PEM fuel cell.

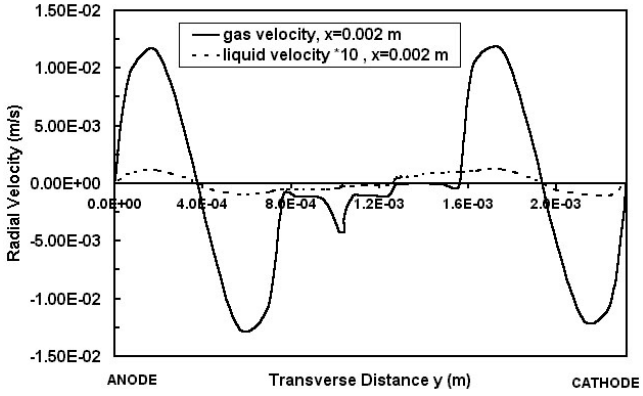

Fig. 5 Profiles of transverse velocities of gas and liquid water in PEM fuel cell, T=353 K at 0.7 cell voltage.

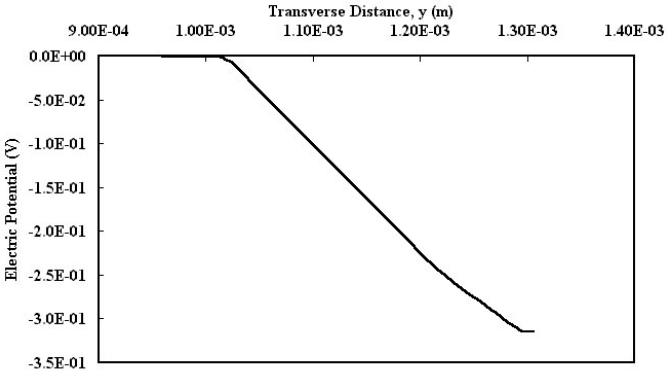

Fig. 8 Electric phase potential (ϕ) V, taking the anode potential as a reference, in the PEM fuel cell, cell potential = 0.8 V, in catalyst layers and membrane

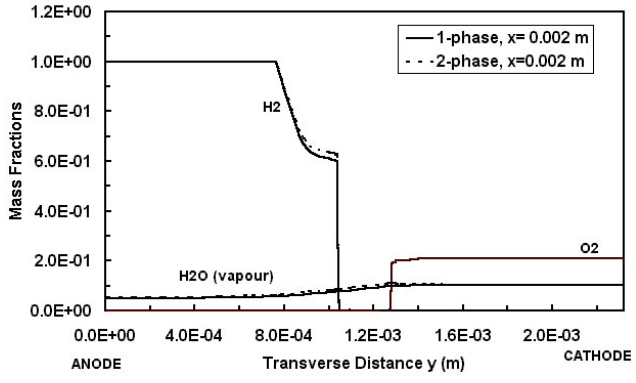

Fig. 6 Transverse profiles of mass fractions of H2, O2 and H2O at an axial distance of 0.002 m, in PEM fuel cell at 353 K.

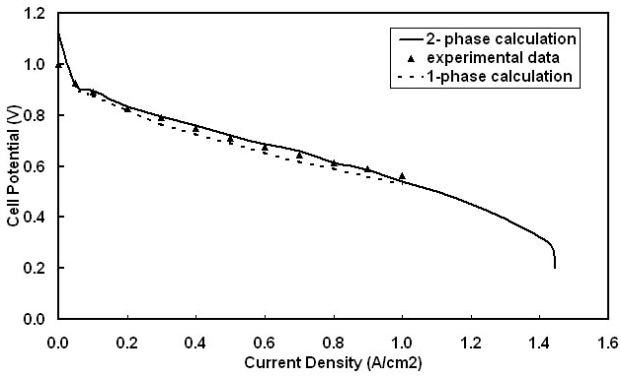

Fig. 9 Predicted cell potential for single and 2-fluid models at T=353 K and the experimental data of Ticianelli et al, 1988 for the PEM fuel cell.

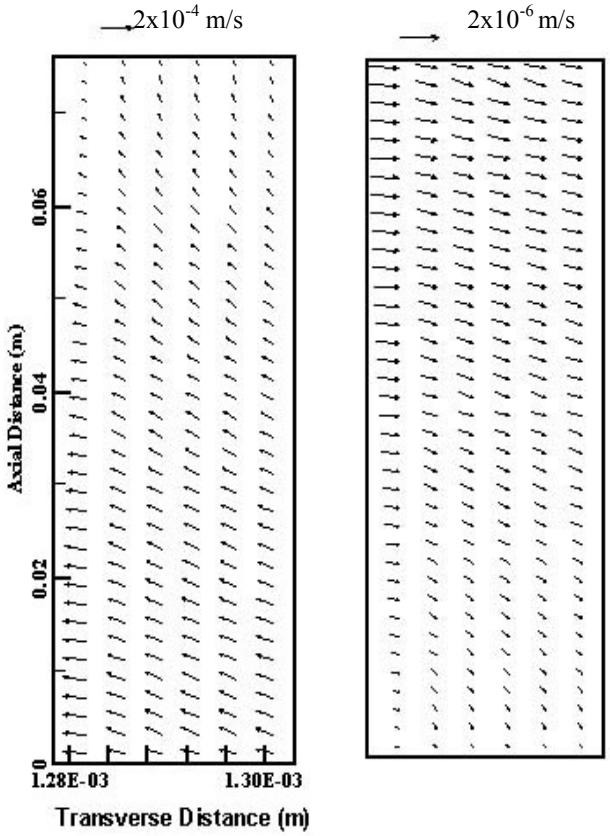

(a) gas velocity (b) liquid velocity

Fig.10 Velocity vector plots, in the cathode catalyst layer and GDL,(a) for the gas and (b) for the liquid water, at 0.8 V cell potential.

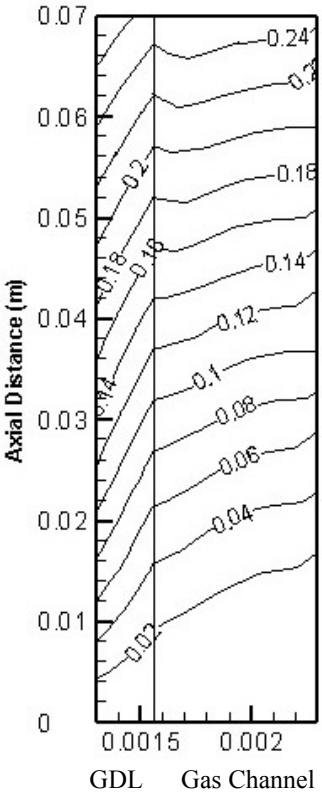

Fig.11 Liquid water volume fraction contours in the cathode, close to the limiting current density at 0.22 V cell potential.